Indian Journal of Pure & Applied Physics
Vol. 64, March 2026, pp. 327-337
DOI: 10.56042/ijpap.v64i3.26842

Modelling and Performance Optimization of Orthogonal MIMO Dielectric Resonator Antenna with Defected Ground Structure

Amsaveni A*, Bharathi M & Megavarshini R

Department of Electronics and communicaton Engineering, Kumaraguru College of Technology Coimbatore 61 049, India

Received: 23rd December 2025; accepted: 3rd February 2026

This research introduces a high-efficiency multiband MIMO antenna system based on Dielectric Resonator Antennas (DRAs) integrated with a Defected Ground Structure (DGS). Designed to operate at 5.6 GHz, 7.3 GHz, and 8.9 GHz, the antenna supports various modern wireless applications, including Wi-Fi, 5G New Radio (NR), Internet of Things (IoT), Vehicle-to-Everything (V2X) communication, and radar technologies. The antenna is built on an FR4 substrate and employs two pentagonal alumina (Al_2O_3) resonators, which contribute to its high radiation efficiency (~90 %). A DGS composed of rectangular slots is incorporated to minimize surface wave propagation and significantly enhance isolation between elements ($|S_{12}| < -35$ dB). Compared to conventional MIMO antenna types such as microstrip patches, slot-based, and metasurface configurations the proposed design offers superior isolation and gain (~5 dBi). Additionally, the orthogonal positioning of the resonating elements effectively reduces mutual coupling, reinforcing its suitability for high-performance, next-generation wireless systems.

Keywords: MIMO antenna, Dielectric resonator antenna (DRA), Defected ground structure (DGS), Mutual coupling, Isolation, Multiband

1 Introduction

With the continuous advancement of wireless communication technologies, there is a growing need for antennas that can deliver high data throughput, wide operational bandwidth, and dependable performance. Multiple-Input Multiple-Output (MIMO) technology has become a fundamental aspect of modern wireless systems due to its potential to enhance channel capacity, optimize spectral utilization, and mitigate the adverse effects of multipath propagation[1-2]. Nevertheless, designing compact MIMO antennas presents a significant challenge: mutual coupling between closely spaced elements. This phenomenon can deteriorate key performance parameters such as isolation, antenna gain, and the overall efficiency of the communication system.

To mitigate the problem of mutual coupling in compact MIMO systems, several isolation enhancement strategies have been studied, such as electromagnetic bandgap (EBG) structures, metamaterials, and defected ground structures (DGS). Among these, DGS has drawn interest due to its usefulness, affordability, and simplicity of use without requiring a major change in the overall size of the antenna[3-4]. DGS efficiently modifies the surface current paths by incorporating intentional discontinuities or patterns in the ground plane. This helps to reduce undesired coupling between antenna elements and improves impedance matching across a wide frequency range.

Dielectric Resonator Antennas (DRAs) have become increasingly popular for use in high-frequency and multiband systems due to their unique benefits such as excellent radiation efficiency, low ohmic losses, and versatile design options[5]. When built using high-permittivity materials like alumina (Al_2O_3), DRAs offer the advantage of compactness without sacrificing performance. Moreover, their physical shape can be tailored to excite multiple resonant modes, making them highly suitable for incorporation into modern MIMO antenna architectures.

In this study, a novel MIMO antenna configuration based on DRAs is presented, featuring a rectangular-slot DGS and orthogonal arrangement of the resonators to enhance isolation and support multiband functionality. The design is implemented on a standard FR4 substrate and is tuned to operate at 5.6 GHz, 7.3 GHz, and 8.9 GHz frequencies relevant to

*Corresponding author: E-mail: amsaveni.a.ece@kct.ac.in

next-generation technologies such as Wi-Fi 6E, 5G New Radio (NR), the Internet of Things (IoT), Vehicle-to-Everything (V2X) communications, and advanced radar applications[6-7].

2 Literature Review

Recent advancements in MIMO antenna research have placed strong emphasis on enhancing key performance parameters such as isolation, gain, and bandwidth through structural innovation. Among the various techniques explored, the use of DGS has proven particularly effective in reducing mutual coupling between antenna elements.

A compact antenna array designed for WLAN applications was reported, where mutual coupling was effectively reduced through geometric optimization. Meanwhile, dielectric resonator antennas have attracted increasing attention due to their excellent radiation characteristics and high permittivity materials[8]. A wideband circularly polarized DRA employing an S-shaped feed slot was presented, offering an efficient solution for space-constrained high-frequency systems[9].

A DRA-based MIMO antenna intended for 5G mm Wave applications was presented[10], where high isolation was achieved through optimized element placement and appropriate material selection. The effectiveness of integrating a defected ground structure for realizing dual-band MIMO operation with enhanced decoupling was demonstrated[11]. For ultra-wideband applications, a compact MIMO antenna incorporating built-in band-rejection characteristics was reported[12], while wideband MIMO designs offering strong isolation across extended frequency ranges were presented[13].

A millimeter-wave MIMO antenna using a combined decoupling structure and common defected ground plane was reported, achieving improved isolation and reduced mutual coupling. The defected ground effectively suppressed surface currents, resulting in enhanced bandwidth and MIMO performance[14].

These studies demonstrate how DGS and DRA technologies can be used to greatly improve MIMO antenna's performance on a variety of wireless communication platforms.

3 Methodology

3.1 Antenna Design

The schematic representation of the proposed MIMO-based DRA antenna, as illustrated in Fig. 1. The MIMO antenna consists of an FR4 substrate (ε_{sub}= 4.4, tan δ = 0.02) along with two pentagon-shaped dielectric resonator antennas made of alumina (Al_2O_3) with a dielectric constant of $\varepsilon_{Alumina}$ = 9.8 and a loss tangent of tan δ = 0.002.

As in Fig. 2, the design incorporates two antennas arranged orthogonally to minimize mutual coupling ($|S_{12}| < -35$ dB), which is significantly lower compared to their alignment in the same direction. Additionally, a Defected Ground Structure (DGS) is introduced beneath the antennas to further improve

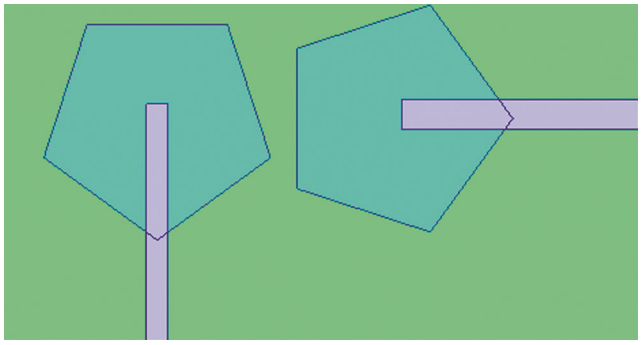

Fig.1 — Top view of the MIMO-based DRA without DGS

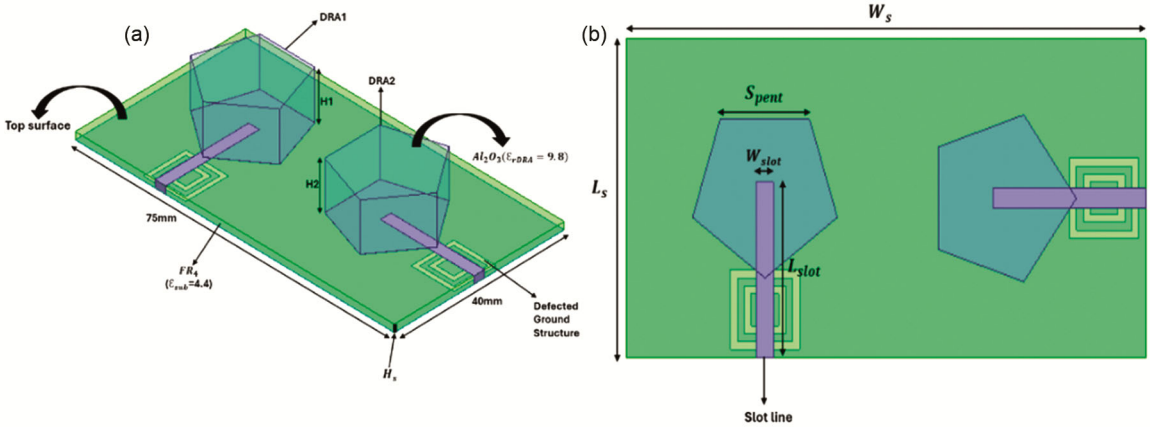

Fig. 2 — Schematic Layout of the MIMO-based DRA (a) Isometric view, and (b) Top view

isolation, suppress surface waves, and enhance overall impedance matching. The rectangular slot DGS modifies the current distribution on the ground plane, leading to improved radiation characteristics and enhanced bandwidth.

To estimate the dimensions of the pentagonal-shaped Dielectric Resonator Antenna and the supporting substrate structure at an operating frequency of 5.6 GHz, we can follow these steps:

$_{\text{Effective}}$ Wavelength of DRA,

$$\lambda_{eff} = \frac{c}{f_o\sqrt{\varepsilon_r}} \quad \ldots (1)$$

This effective wavelength helps define the approximate DRA dimensions, which are typically a fraction (about λ/4 to λ/2) depending on the mode.

Assuming the pentagonal base area supports a TE mode.

$$\text{Effective Height(H1, H2)} \cong \frac{\lambda_{eff}}{4} \quad \ldots (2)$$

$$\text{Base side (Spent)} \cong \frac{\lambda_{eff}}{2.5} \quad \ldots (3)$$

A slot line is etched on the ground plane beneath each DRA to provide coupling. As shown in Table1, the slot has optimized dimensions of: Slot length L_{slot} ≈ 8–10 mm and Slot width W_{slot} ≈ 1.5mm. This coupling scheme ensures wide bandwidth and good impedance matching. The feeding structure is aligned orthogonally for the two DRAs to reduce mutual coupling.

3.2 Mathematical Modelling and Analytical Representation

To better understand and predict the electromagnetic behaviour of the proposed MIMO Dielectric Resonator Antenna (DRA) with Defected Ground Structure (DGS), analytical modelling based on Maxwell's equations is essential. The time-harmonic field relations governing the antenna can be written as:

$$\nabla \times E = -j\omega\mu H, \qquad \nabla \times H = j\omega\varepsilon E \quad \ldots (8)$$

Within the dielectric resonator, the electric field must satisfy the vector Helmholtz equation:

$$\nabla^2 E + k^2 E = 0 \quad \ldots (9)$$

where $k = \omega\sqrt{(\mu\varepsilon)}$ is the propagation constant inside the dielectric. For alumina (εr = 9.8), this value becomes considerably higher than that in free space, allowing compact physical dimensions while maintaining resonance.

For any resonant mode in the DRA, the propagation constants satisfy the eigenvalue relationship:

$$kd^2 = kx^2 + ky^2 + kz^2 \quad \ldots (10)$$

Considering the pentagonal shape of the resonator, an equivalent circular radius (aeq) can be derived from the pentagon's area Ap as:

$$aeq = \sqrt{(Ap/\pi)} = \sqrt{((5Sp^2/4\pi)\tan(54°))} \quad \ldots (11)$$

The fundamental resonant frequency of the DRA can then be approximated as:

$$fr = c / (2\pi aeq\sqrt{(\varepsilon r - 1)})\ Fmnp \quad \ldots (12)$$

where Fmnp represents the mode-specific eigenvalue, c is the velocity of light, and εr is the relative permittivity of the dielectric medium.

Table 1 — Optimized Dimensions of Different Parameters

Parameter	Symbol	Approx. Value
Operating Frequency	f_o	5.6 GHz
Effective Wavelength	λ_{eff}	14.04 mm
DRA Height	H_1, H_2	3.5 mm
Pentagon Side Length	Spent	5.6 mm
Substrate Length	L_s	75 mm
Substrate Width	Ws	40 mm
Slot Length	L_{slot}	8–10 mm
Slot Width	Wslot	1.5 mm
Substrate Thickness (FR4)	H_s	~1.6 mm

3.3 Equivalent Circuit Model of DGS

A single DGS cell is commonly modelled as a resonant LC element that, when placed as a shunt to ground, forms a stopband around f_c. This simple circuit (Fig. 3) captures how the etched slot perturbs surface currents and creates isolation/attenuation in specific frequency bands.

The Defected Ground Structure can be described by an equivalent LC circuit, where the etched slot adds both inductive and capacitive effects to the ground plane. The impedance of a single DGS cell is expressed as:

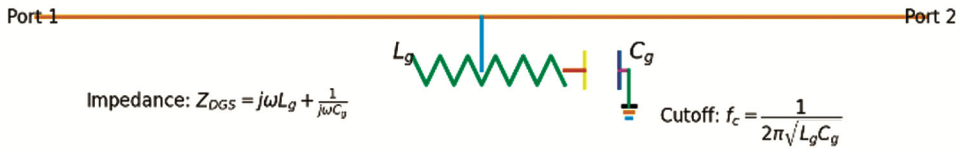

Fig. 3 — Equivalent circuit of DGS

$$Z_{DGS} = j\omega Lg + 1/(j\omega Cg) \quad \ldots (13)$$

and the cutoff frequency corresponding to the stopband created by the DGS is:

$$fc = 1 / (2\pi\sqrt{(LgCg)}) \quad \ldots (14)$$

This modification in the ground impedance alters surface current paths, suppresses unwanted coupling, and improves the impedance bandwidth of the antenna.

The mutual coupling coefficient (kc) between the two radiating elements can be derived from the overlap of their near-field regions as:

$$kc = \int V E1 \cdot E2^* \, dV / \sqrt{(\int V |E1|^2 \, dV \int V |E2|^2 \, dV)} \quad \ldots (15)$$

A lower value of kc indicates improved isolation. In practical design, the transmission coefficient (S_{12}) is related to the coupling coefficient by:

$$|S_{12}| \approx 20 \log10 |kc| \quad \ldots (16)$$

The overall radiation efficiency of the DRA is determined by the ratio of radiated power to total input power:

$$\eta r = Prad / (Prad + Ploss) = 1 / (1 + Ploss/Prad) \quad \ldots (17)$$

where Ploss includes dielectric, conductor, and surface-wave losses. Incorporating the DGS reduces these losses by redistributing surface currents.

The total gain of the antenna can be formulated as:

$$G = \eta r \times D = \eta r \times (4\pi Umax/Pin) \quad \ldots (18)$$

where D is the directivity, Umax is the maximum radiation intensity, and Pin denotes the total input power.

The above formulations establish a direct mathematical connection between antenna geometry, dielectric properties, and electromagnetic performance. The derived expressions clarify how the combination of DRA and DGS geometries enhances isolation, gain, and impedance matching.

4 Results and Discussion

The simulated performance of the proposed pentagon-shaped MIMO Dielectric Resonator Antenna (DRA) with and without the integration of a DGS. The analysis is based on key antenna parameters such as return loss ($|S_{11}|$), bandwidth, and resonance behavior over the frequency range of 1 GHz to 10 GHz. The comparison aims to evaluate the effectiveness of the DGS in enhancing impedance matching, multiband performance, and minimizing mutual coupling. Simulation results are obtained using Ansys HFSS.

4.1 Return Loss Comparison with and without DGS

Figure 4 presents the simulated $|S_{11}|$ parameters of the proposed MIMO DRA antenna in two configurations: In the absence of DGS (Fig. 4(a)), the antenna demonstrates limited impedance matching and shallow resonances. The most prominent resonance appears around 5.6 GHz, with a return loss of approximately -13 dB, while the remaining resonant dips are less defined and exhibit relatively poor matching (above -10 dB). The bandwidth is narrow, and reflection is higher, indicating significant power loss due to poor coupling and impedance mismatch.

By incorporating a concentric Defected Ground Structure around the slot lines (Fig. 4 (b)), the return loss performance improves significantly. Strong resonant dips are observed at 5.6 GHz, 7.3 GHz, and 8.9 GHz, with return loss values reaching -22.23 dB, -14.68 dB, and -13.64 dB, respectively. This confirms better impedance matching and energy transfer at multiple operating bands.

The DGS effectively alters the surface current distribution, thereby: Suppressing surface waves, enhancing isolation between antenna elements and expanding bandwidth at each resonant frequency. This improvement is evident from the deeper nulls in the $|S_{11}|$ plot and the formation of multiple well-separated resonances.

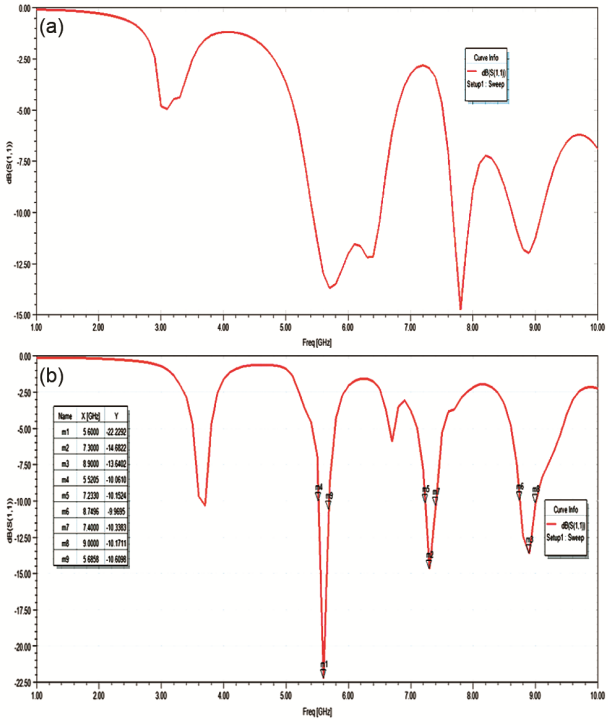

Fig. 4 — $|S_{11}|$ graph (a) without DGS (b) with DGS

4.2 Radiation pattern

The radiation characteristics of the proposed antenna at its resonant frequencies are illustrated in Fig. 5 and analysed as follows.

At 5.6 GHz, the antenna exhibits a directional radiation pattern with noticeable asymmetry in gain across various angles and azimuthal cuts (ϕ=0°,90°,180°). The presence of distinct peaks and nulls confirms that the radiation is not uniformly distributed, indicating a non-omnidirectional nature.

At 7.3 GHz, the radiation behaviour remains directional, with relatively broad main lobes in the ϕ=0° and ϕ=90° planes. However, the pattern corresponding to ϕ=180° reveals a deep null near −180°, signifying limited radiation in that direction and sharper beam shaping.

At 8.9 GHz, the antenna presents a more complex and sharply directional pattern, featuring multiple lobes and deep nulls across all three phi planes. This behaviour reflects a more intricate field distribution and higher angular sensitivity, although the overall gain is reduced compared to the lower resonant frequencies. Such characteristics are typical of higher-order mode excitation and confirm the antenna's suitability for selective, angle-dependent communication paths.

4.3 Gain

Figure 6 presents the 3D gain patterns of the proposed MIMO DRA at 5.6 GHz, 7.3 GHz, and 8.9 GHz. These plots highlight the antenna's radiation behavior across space, offering a clear view of its directional strength and coverage at each frequency.

At 5.6 GHz, the antenna achieves a peak gain of around 3.31 dB with a moderate directional radiation pattern. The forward lobe dominates, indicating focused energy transmission. Brighter regions (yellow and red) reflect higher gain, while cooler tones (blue and green) indicate weaker radiation, confirming efficient directional performance.

At 7.3 GHz, the antenna exhibits its highest peak gain of 4.59 dB across the three operating bands. Radiation becomes more focused, with intensified red regions indicating stronger, concentrated signal strength. The narrower main lobe reflects improved directivity, making the design well-suited for applications that demand precise beam targeting and enhanced isolation.

At 8.9 GHz, the antenna shows a more intricate and less symmetrical radiation pattern, reaching a peak gain of 3.79 dB. The presence of multiple lobes and varying field strength points to the excitation of higher-order modes. This broader and more irregular energy distribution indicates greater angular sensitivity, which can be beneficial for applications requiring directional diversity or adaptive beam steering.

Overall, the gain plots confirm that the antenna delivers reliable directional radiation with frequency-

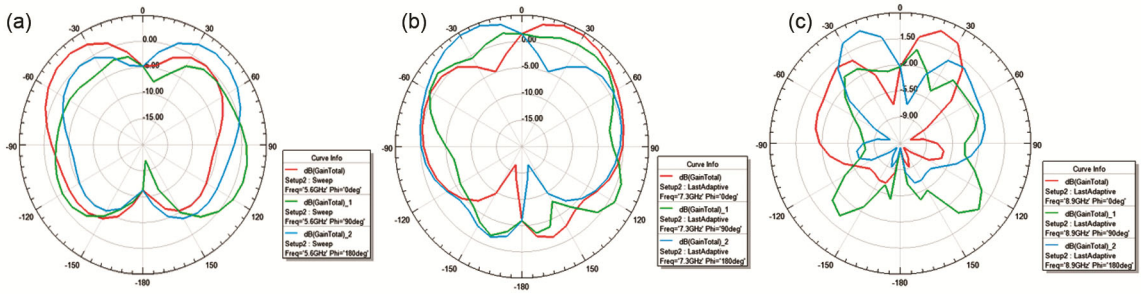

Fig. 5 — Simulation results of MIMO DRA - Radiation pattern at (a) 5.6GHz (b) 7.3GHz, and (c) 8.9GHz

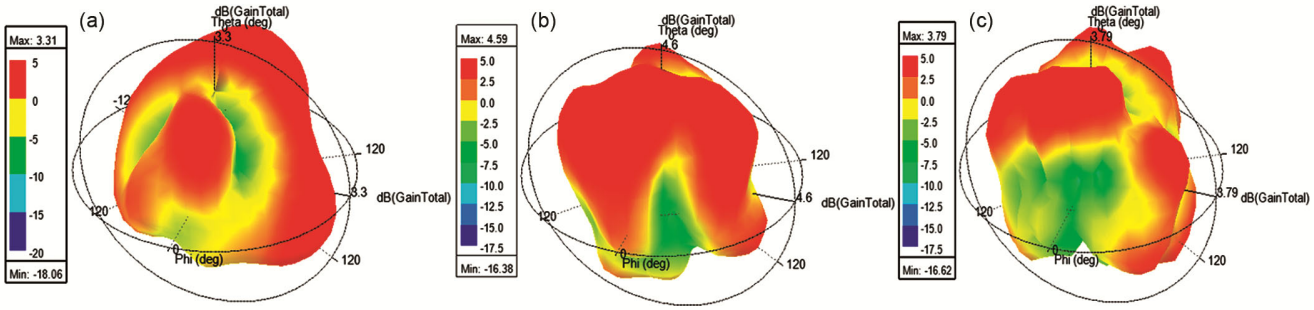

Fig. 6 — Simulation results of MIMO DRA – Gain at (a) 5.6GHz (b) 7.3GHz, and (c) 8.9GHz

dependent behavior. The design maintains solid gain performance across all three resonant frequencies, validating its suitability for multiband and directional MIMO systems.

4.4 Polarization

The axial ratio (AR) is a key parameter used to determine the polarization of an antenna. As shown in Table 2, AR values across different frequencies and angular orientations indicate that the proposed antenna primarily exhibits linear polarization. At 5.6 GHz, the AR values are consistently high, ranging from 15.44 dB to 21.96 dB, confirming strong linear polarization. At 7.3 GHz, a slightly lower AR of 4.91 dB is observed at ϕ=90∘, θ=90∘, suggesting elliptical polarization in that specific direction, while the other orientations still maintain linear with ARs above 12 dB. At 8.9 GHz, all AR values exceed 13 dB, with the highest reaching 35.06 dB. Overall, the AR value confirms that the antenna predominantly radiates in a linearly polarized manner across all operating bands.

Figure 7 presents the vector electric field distribution of a MIMO DRA structure, providing insight into the polarization characteristics of the antenna. The direction and alignment of the E-field vectors suggest that the radiated wave predominantly oscillates in a single plane, which is indicative of linear polarization.

The relatively higher axial ratio of 4.91 dB at 7.3 GHz is attributed to partial excitation of the orthogonal field components and a slight amplitude and phase imbalance between them, resulting from the modal distribution and coupling characteristics of the dielectric resonator at this resonance.

Table 2 — AR(dB) at different frequencies

Freq (GHz)	AR in dB ϕ=0° θ=0°	ϕ=90° θ=90°	ϕ=180° θ=180°	Polarization Type
5.6	18.49	15.44	21.96	Linear
7.3	12.13	4.91	14.85	Mostly Linear, Some Ellipticity at 90°
8.9	35.06	13.10	23.09	Linear

4.5 Field Distribution

Figure 8 illustrates the simulated E-field distribution of the antenna structure. The colour gradient indicates the magnitude of the E-field, with red regions representing high E-field strength and blue regions representing low E-field strength. The high E-field concentrations around the feed lines and radiating elements suggest efficient radiation from the antenna.

The E field distribution indicates that the antenna elements are resonating effectively. The separate E-field concentrations around the two antenna elements are a positive sign for the MIMO characteristics of the antenna.

4.6 MIMO Performance Metrices

4.6.1 Isolation

From Fig. 9, the magnitude of S_{21} indicates that the proposed MIMO Dielectric Resonator Antenna (DRA) maintains excellent isolation and low mutual coupling over most of the operating band. The parameter $|S_{21}|$ stays below 0.01 across key frequency

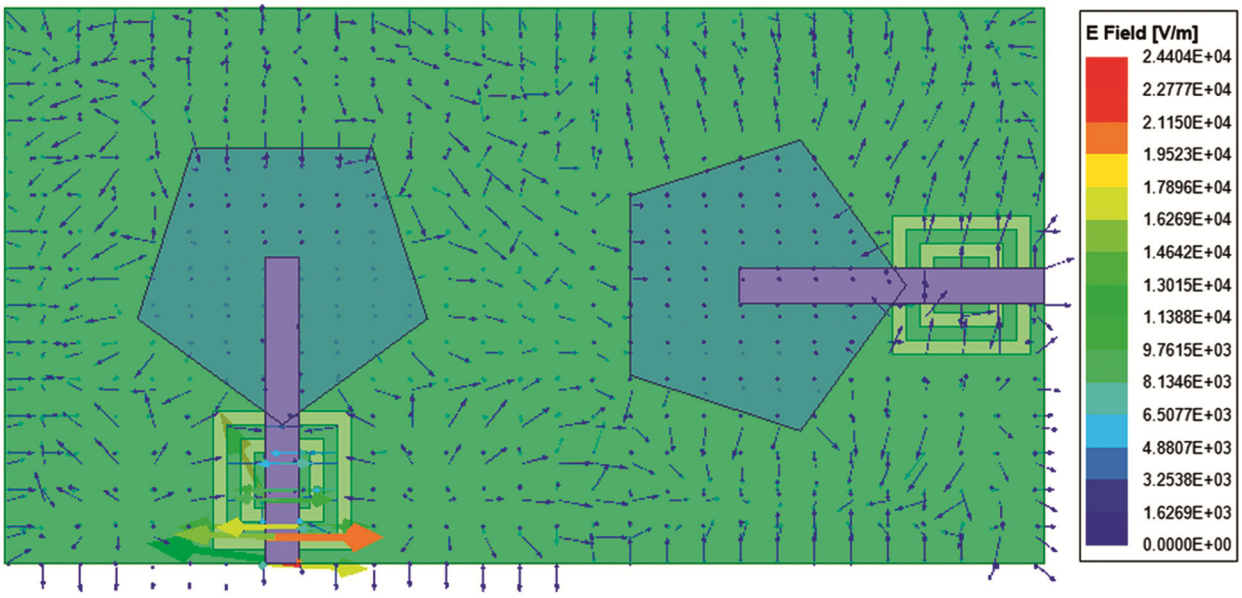

Fig. 7 — Vector Electric field distribution

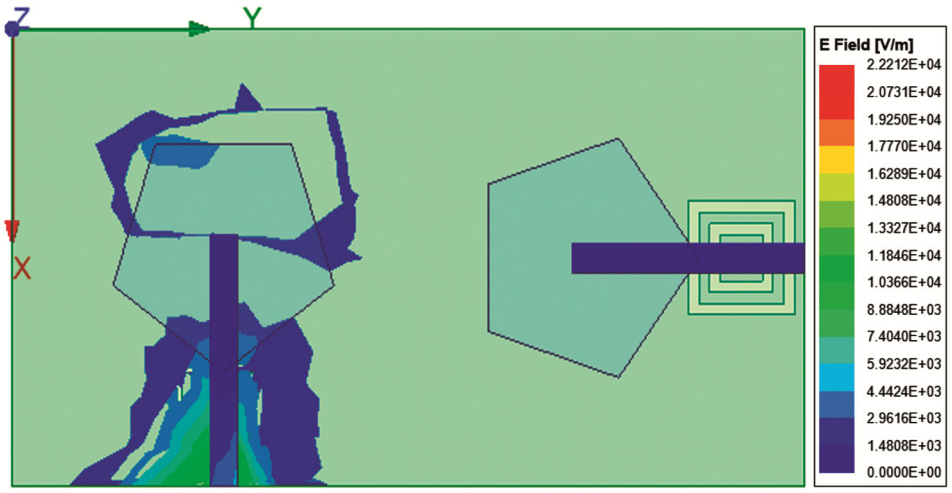

Fig.8 — Simulated E-field distribution of the Proposed Antenna Structure

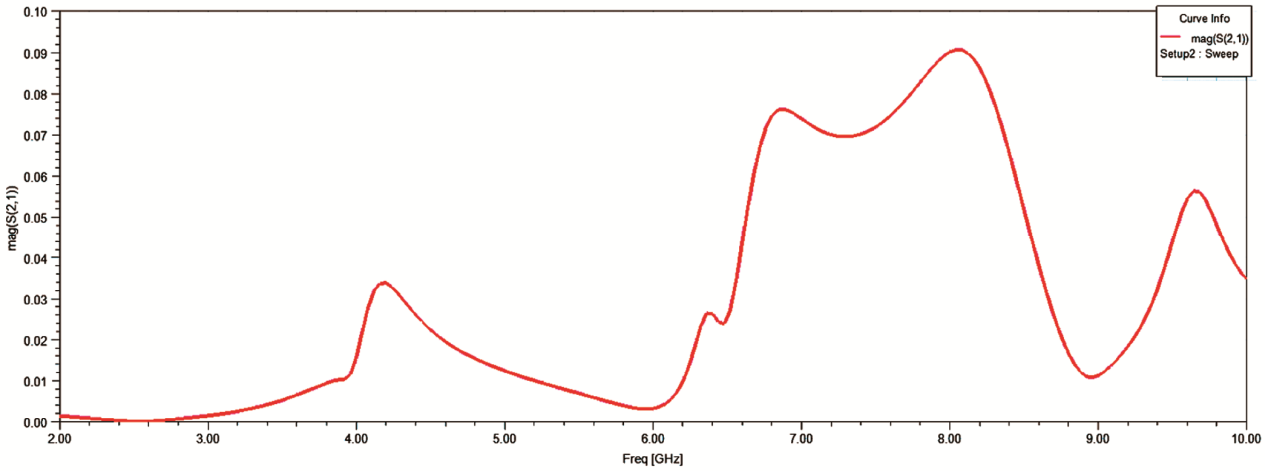

Fig. 9 — S_{21} plot (linear Scale) for the Proposed Antenna

ranges, corresponding to isolation levels better than –40 dB, which is ideal for MIMO systems. Even in frequency regions with slight increases in coupling, isolation remains within acceptable limits. This confirms the antenna's capability to suppress mutual coupling, improve diversity performance, and support reliable wireless communication.

Table 3 compares the simulated isolation performance (S_{21}) of the proposed MIMO DRA antenna with and without the incorporation of the defected ground structure (DGS). Without DGS, the isolation remains in the range of −18 to −22 dB across the three resonant frequencies.

With the introduction of DGS, the isolation improves significantly to better than −35 dB at all operating bands, reaching below −40 dB at higher frequencies. This clearly demonstrates the effectiveness of the DGS in suppressing mutual coupling and enhancing MIMO performance.

Table 3 — Comparison of isolation performance with and without DGS

Resonant Frequency	Without DGS (S_{21}) (dB)	With DGS(S_{21}) (dB)
5.6 GHz	≈ −18	< −35
7.3 GHz	≈ −20	< −38
8.9 GHz	≈ −22	< −40
Average Isolation (S_{21})	−18 to −22	< −35

4.6.2 Total Active Reflection Coefficient (TARC)

Computing the Total Active Reflection Coefficient (TARC) in MIMO systems is crucial as it provides a comprehensive measure of reflection and mutual coupling when multiple ports are excited simultaneously

$$TARC = \sqrt{\frac{|S_{\{11\}}+S_{\{12\}}|^2+|S_{\{21\}}+S_{\{22\}}|^2}{2}} \quad \ldots (19)$$

The analysis of TARC from Fig. 10 demonstrates the antenna's effective multiband operation within the 1-10 GHz frequency range. Several distinct dips in the

dB10(TARC) plot indicate well-matched operating bands, showcasing the antenna's ability to minimize reflected power and ensure efficient signal transmission.

These low TARC values across specific frequency ranges highlight the antenna's potential for robust MIMO performance, making it a promising candidate for applications requiring multiband operation and efficient power transfer.

4.6.3 Envelope Correlation Coefficient (ECC)

The Envelope Correlation Coefficient (ECC) is crucial in MIMO antenna systems as it quantifies the level of correlation between radiation patterns of different antenna elements.

$$ECC = \frac{\left|S_{\{11\}}{}^{*}\, S_{\{12\}} + S_{\{21\}}{}^{*} S_{\{22\}}\right|^2}{\left(1 - \left|S_{\{11\}}\right|^2 - \left|S_{\{21\}}\right|^2\right)\left(1 - \left|S_{\{22\}}\right|^2 - \left|S_{\{12\}}\right|^2\right)} \quad \ldots (20)$$

For efficient MIMO operation, the envelope correlation coefficient (ECC) should ideally approach zero. In practice, ECC values below 0.01 (corresponding to dB10(ECC) < −20 dB) are considered excellent and indicate highly uncorrelated radiation characteristics. From Fig. 11, it is observed that the envelope correlation coefficient at the resonant frequencies remains below −30 dB, indicating excellent MIMO diversity performance. This demonstrates minimal signal correlation between antenna elements, ensuring high MIMO capacity and robust performance.

4.6.4 Diversity Gain (DG)

$$DG = 10\sqrt{1 - (ECC)^2} \quad \ldots (21)$$

Diversity Gain (DG) is essential in MIMO systems as it measures the improvement in signal

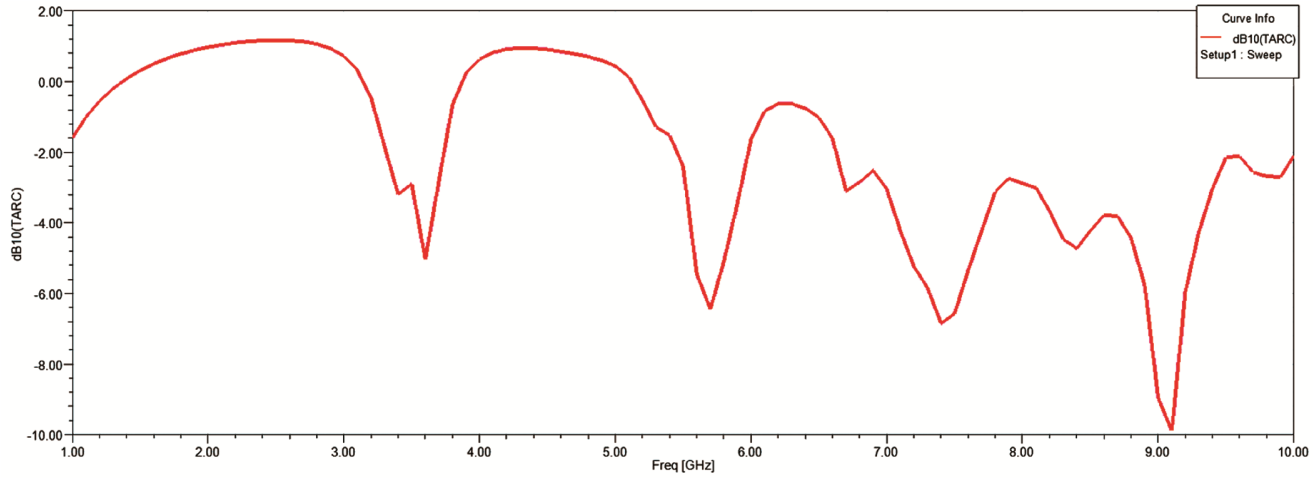

Fig. 10 — TARC plot for the Proposed Antenna

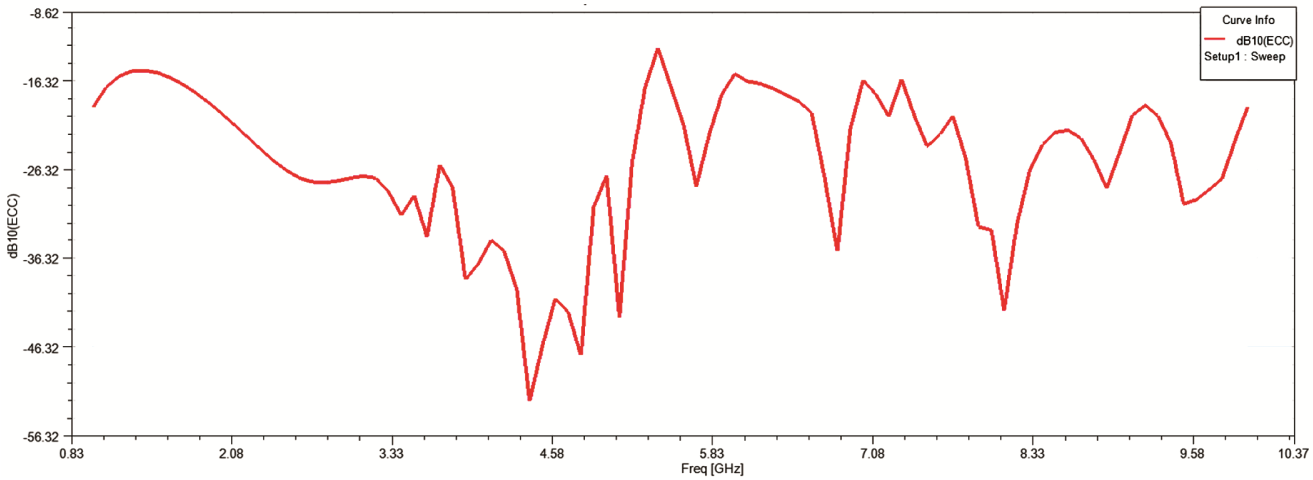

Fig. 11 — dB10 ECC plot for the Proposed Antenna

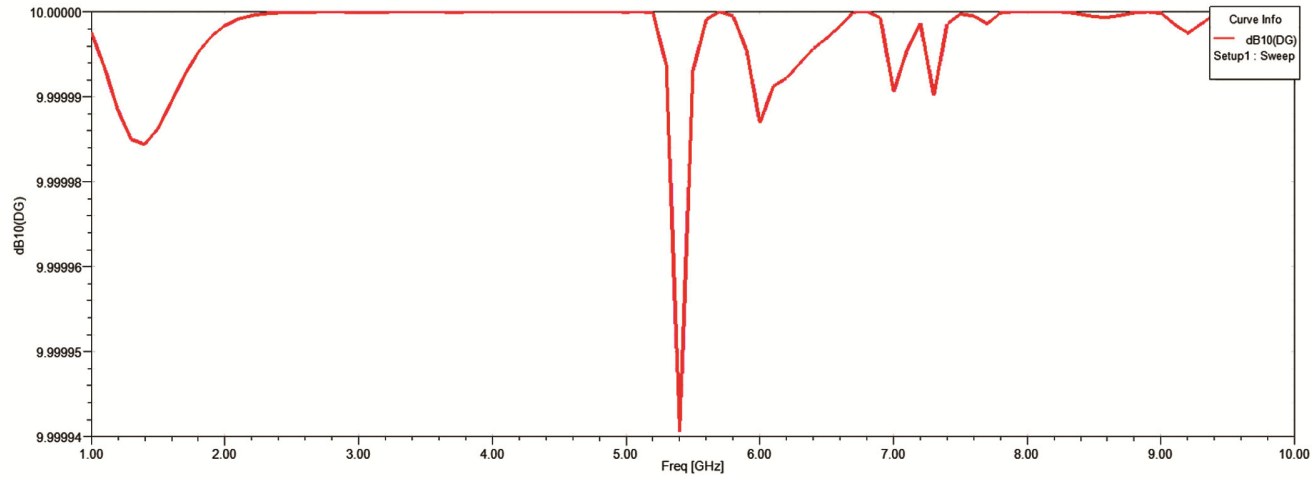

Fig.12 — DG plot for the Proposed Antenna

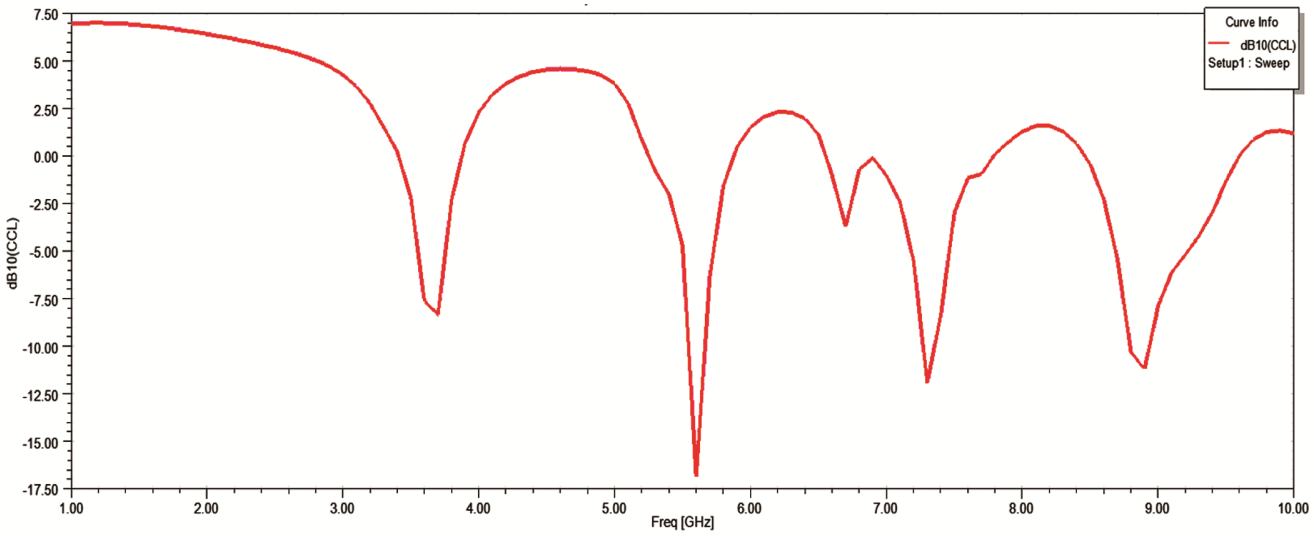

Fig.13 — CCL plot for the Proposed Antenna

reliability due to multiple antennas mitigating fading effects.

As shown in Fig. 12, the diversity gain remains close to 10 dB across most of the operating frequency bands, indicating near-ideal diversity performance of the proposed MIMO antenna. However, a sharp dip in DG around 5.5 GHz indicates a potential reduction in diversity at this specific frequency.

4.6.9 Channel Capacity Loss (CCL)

Channel Capacity Loss (CCL) is crucial in MIMO systems as it quantifies the reduction in achievable data rate due to correlation between antenna elements.

$$CCL = -\log_2\left(1 - S_{\{11\}}^2 - S_{\{12\}}^2\right) \quad \ldots (22)$$

As illustrated in Fig. 13, the channel capacity loss remains close to the ideal value of zero across most of the operating frequency range. The observed low CCL values (below the commonly accepted limit of 0.4 bits/s/Hz) indicate minimal capacity degradation and confirm efficient MIMO channel performance. Several distinct dips in the plot indicate frequency bands with reduced channel capacity loss, highlighting the antenna's potential for efficient MIMO operation within these specific ranges. Conversely, higher CCL values at other frequencies suggest significant capacity reduction. The antenna exhibits suitable MIMO performances in the low CCL bands.

The proposed antenna is primarily intended for narrowband or channel-specific applications, such as radar sensing, V2X control links, and sub-band 5G/Wi-Fi channels. Accordingly, the focus of this work is on achieving high isolation, multiband selectivity, and compact MIMO integration,

Table 4 — Overall Performance of Proposed antenna

Performance Metric	Measured Value / Description
Resonant Frequencies (GHz)	5.6, 7.3, 8.9
Operating Bands (GHz)	5.52–5.68, 7.23–7.40, 8.74–9.00
Bandwidth (MHz)	16 / 17 / 26
Return Loss (dB)	–22.23 (5.6 GHz), –14.68 (7.3 GHz), –13.64 (8.9 GHz)
Gain (dBi)	3.38, 4.59, 3.79
Isolation loss, S_{21}	< -35 dB
TARC	Multiple dips below –10 dB across operating bands
ECC	< 0.01 (across 0.8–10 GHz)
Diversity Gain (DG)	~10 dB (dip near 5.5 GHz)
Channel Capacity Loss (CCL)	< 0.5 bits/s/Hz in most bands
Polarization	Linear across all bands (slight ellipticity at 7.3 GHz, AR = 4.91 dB at one angle)
Axial Ratio (AR)	> 13 dB (except one case at 7.3 GHz: 4.91 dB)

Table 5 — Comparison with existing works

Metric	Patel *et al.*[15]	Rai *et al*[16]	Alanazi & Khamas[17]	Proposed Work
Operating Bands (GHz)	3.72 & 4.75	Wideband	28 & 38	5.6, 7.3 & 8.9
Isolation (S_{21})(dB)	> 20	> 20	~27–44	< −35
Peak Gain (dBi)	9.12 & 8.58	~4.3	~6.2 & 7.57	3.38–4.59
ECC	~0.042	Within acceptable limits	Very low	Very low (≪ 0.1)
Diversity Gain (DG) (dB)	~9.99	Acceptable	Close to 10	≈10
CCL	< 0.2 bits/s/Hz	Acceptable	Very low	Very Low

rather than targeting ultra-wideband operation. The overall performance of the antenna is listed in Table 4.

Table 5 compares the proposed multiband MIMO DRA with recent works in literature. The proposed antenna demonstrates high isolation (< −35 dB) across the operating bands, which is superior to earlier studies[15,16]. Although the peak gain is lower than that reported[15,17], it remains within acceptable limits for compact multiband DRA implementations. The antenna also exhibits excellent MIMO performance with low ECC, near-ideal DG (≈ 10 dB), and low CCL.

5 Conclusion

The proposed MIMO Dielectric Resonator Antenna with Defected Ground Structure exhibits enhanced performance across multiple frequency bands. With resonant frequencies at 5.6 GHz, 7.3 GHz, and 8.9 GHz, and mutual coupling reduced to below –35 dB, the antenna ensures strong isolation and reliable MIMO functionality. The DGS integration significantly improves impedance matching, bandwidth, and gain while minimizing surface wave effects. The proposed antenna is intended for narrowband or channel-specific applications, such as radar sensing, V2X control links, and sub-band 5G/Wi-Fi channels. Fabrication of the proposed antenna and its experimental validation using a vector network analyzer and an anechoic chamber are planned as part of future work.

References

1 Numan A B, Sadat S M S, Reza S A & Numan A D N, "A defected ground structure for isolation enhancement in a printed MIMO antenna system," *7th European Conference on Antennas and Propagation (EuCAP)*, 2013 pp. 2123–2126.

2 Luo C-M, Hong J-S, & Zhong L-L, *IEEE Antennas Wireless Propag Lett*, 14 (2015) 1766.

3 Amsaveni A, Bharathi M & Swaminathan J N, *Microsyst Technol*, 25 (6) (2019) 2273.

4 Amsaveni A & Bharathi M, In *2021 International Conference on Advancements in Electrical, Electronics, Communication, Computing and Automation (ICAECA)*, October 2021 pp. 1-5.

5 Mishra M, Pattnaik C S, Behera S K & Mishra D K, *3rd URSI Atlantic and Asia Pacific Radio Science Meeting (AT-AP-RASC)*, 2022 pp. 1–4.

6 Amsaveni A, Harish L, Rashmi S & Kaiser A, *Int J Vehicle Inform Commun Syst*, 9 (1) (2024) 103.

7 Amsaveni A, Bharathi M, Tharun R B & Madhavan T, *Ind J Pure Appl Phys*, 63 (10) (2025) 952.

8 Dash U & Pattnaik S S, *Microw Optic Technol Lett*, 60 (2) (2018) 297.

9 Mukherjee B, Patel P & Mukherjee J, *J Electromagnet Waves Appl*, 34 (9) (2020) 1095.

10 Zhang Y, Deng J-Y, Li M-J, Sun D & Guo L-X, *IEEE Antennas Wireless Propag Lett*, 18 (2019) 747.

11 Himaja M, Mondal D, Yuvaraj S & Kartikeyan M V, "Design and Analysis of a Dual Band MIMO Antenna for Improved Isolation using the Defected Ground Structure,"

IEEE Wireless Antenna and Microwave Symposium (WAMS), 2022 pp. 1–5.

12 Wang B., Wang H., & Yu H., "A very compact UWB-MIMO antenna with band-notched characteristic," *IEEE International Workshop on Electromagnetics, Applications and Student Innovation Competition*, 2013 pp. 124–127.

13 Kumar A, Sharma P & Giri S S, "Compact MIMO antenna system with high isolation for ultra-wideband applications," *International Conference on Wireless Communications, Signal Processing and Networking*, 2017 pp. 2496–2498.

14 Tiwari P, Gahlaut V, Kaushik M, Shastri A, Arya V, Elfergani I & Rodriguez J, *Technolog*, 11 (5) (2023) 142.

15 Patel A, Upadhyaya T, Girjashankar P R, Swati M V & Kumar O P, *Sci Rep*, 15 (2025) 10653.

16 Rai J K, Dwivedi A K, Singh V, *et al.*, *Sci Rep*, 15 (2025) 9648.

17 Alanazi M D & Khamas S K, *Sensors*, 22 (13) (2022) 5056.